

Investigation of the ^{19}Na nucleus via resonance elastic scattering

B.B. Skorodumov,* P. Boutachkov, A. Aprahamian,
J.J. Kolata, L.O. Lamm, M. Quinn, and A. Woehr
*Institute of Structure and Nuclear Astrophysics,
University of Notre Dame, Notre Dame, IN 46556*

G.V. Rogachev

*Institute of Structure and Nuclear Astrophysics,
University of Notre Dame, Notre Dame, IN 46556 and
Physics Department, Florida State University, Tallahassee, FL 32306*

(Dated: July 3, 2018)

Abstract

The structure of the unbound proton-rich isotope ^{19}Na was studied in resonance elastic scattering of a radioactive ^{18}Ne beam on a proton target using the thick-target inverse-kinematics method. The experiment covered from 0.5 meV to 2.7 meV in c.m.s. Only one state of ^{19}Na (the second excited state) was observed. A combined R -matrix and potential model analysis was performed. The spin and parity assignment of this second excited state was confirmed to be $1/2^+$. We show that the position of the $1/2^+$ state significantly affects the reaction rate through that state but the total reaction rate remains unchanged since the $^{18}\text{Ne}(2p,\gamma)$ proceeds mostly via the ground and first excited states in ^{19}Na at stellar temperatures.

*Electronic address: bskorodo@nd.edu

I. INTRODUCTION

The structure of light exotic isotopes is currently one of the major topics in nuclear physics. Properties of light neutron-deficient isotopes are not as well known as the properties of their neutron-rich mirrors. The Coulomb interaction leads to proton unbound states in neutron-deficient nuclei even though the corresponding states are bound in the mirror nuclei. Decay properties of these nuclei yield additional information about their structure as well as the structure of states in the mirror nuclei. One such example is ^{19}Na , a proton drip-line isotope which is unbound with respect to proton emission by only 321 keV. It was first observed by Cerny et al. [1] and until very recently only its mass and the excitation energy of its first excited state were experimentally known. The lack of experimental information on the level structure of ^{19}Na is due to technical difficulties related to the population of the excited states of this rather exotic nucleus with three fewer neutrons than the stable sodium isotope ^{22}Na . The second excited state in ^{19}Na was recently observed in a $^{18}\text{Ne}+p$ elastic scattering experiment [2] in which a narrow excitation energy range (0.4 - 1.1 MeV) was covered. The original goal of this work was to extend our knowledge of the structure of ^{19}Na to higher excitation energies (up to 2.7 MeV) using the resonance elastic scattering of a radioactive beam of ^{18}Ne on protons (the upper limit in excitation energy is implied by the maximum possible energy of ^{18}Ne beam that can be produced at ISNAP [3]). During the review stage of this manuscript new study of the ^{19}Na nucleus was published from the study at SPIRAL (GANIL) by Oliveira et al. [4]. In this work, the spectrum of ^{19}Na was measured up to excitation energy of 5.7 MeV at one angle (180°) using the Thick Target Inverse Kinematics (TTIK) technique [5]. Two additional resonances at higher excitation energies were found in [4]. In addition, two broad peaks at $E_{cm} \approx 2.4$ and 3.1 MeV were observed. It was pointed out by the authors in [4] that these peaks can originate from process other than elastic scattering. The first peak is in the energy range of our experiment and should be populated if the origin of this peak is in fact related to elastic scattering. Therefore, it is of interest to compare our data, obtained at a lower beam energy and different angles with the data from [4]. The structure of low lying resonances in ^{19}Na also has some astrophysical interest. It was shown in [6] that at certain stellar temperature and density conditions two-proton capture reaction on ^{18}Ne can play an important role in bridging the waiting point nucleus ^{18}Ne and provide continuous flow between the CNO and

the Fe-Ni mass region in the rp -process. The $^{18}\text{Ne}(2p,\gamma)$ reaction rate was recalculated taking into account new information on the excitation energy of the second excited state.

In the following sections, we present the results of resonance elastic scattering of ^{18}Ne on protons, discuss the structure of the ^{19}Na nucleus, and finally discuss the influence of a $1/2^+$ state on two-proton capture reaction rate on the ^{18}Ne nucleus.

II. EXPERIMENT

The experiment was carried out at the TwinSol radioactive nuclear beam facility [3] of ISNAP (Institute of Structure and Nuclear Astrophysics) at the University of Notre Dame. A beam of ^{18}Ne was produced via the $^3\text{He}(^{16}\text{O},^{18}\text{Ne})n$ reaction. The experimental setup is shown in Fig. 1. A primary beam of ^{16}O with an average intensity of 230 electrical nA and an energy of 80 MeV was incident on a 2.5 cm long gas cell containing ^3He gas at a pressure of 1 atm. A Faraday cup placed after the gas cell was used to stop the primary beam and to measure its intensity. Two superconductive solenoids acted as thick lenses to separate the ^{18}Ne beam from other reaction products. The magnetic rigidity of the first superconductive solenoid was set to focus $^{18}\text{Ne}^{+9}$ ions with an energy of 57 MeV onto a $10\ \mu\text{g}/\text{cm}^2$ C stripping foil as shown in Fig. 1, while the second solenoid focused fully-stripped $^{18}\text{Ne}^{+10}$ ions onto the secondary target. The different rigidities of the two solenoids allowed for a much better separation of ^{18}Ne from other reaction products. The ^{18}Ne ions were focused onto a 1 cm (diameter) spot at the secondary target position. Under these conditions, a ^{18}Ne beam was obtained with an intensity of about 10^4 pps, an energy of 56.3 MeV, and an energy spread of 3.2 MeV full width at half maximum (FWHM). The desired ^{18}Ne ions made up only 2% of the secondary beam; the main contamination was ^{16}O (see Fig. 2). Polyethylene (CH_2) foil was used as the secondary target. Its thickness of ($5.52\ \text{mg}/\text{cm}^2$) was chosen to stop the ^{18}Ne ions completely. The Thick-Target Inverse-Kinematics (TTIK) technique [5] was used to obtain an excitation function for resonance elastic scattering. This method is based on the large differences of specific energy losses for heavy ions (^{18}Ne) and protons. Protons backscattered by ^{18}Ne penetrate the target and lose only a small fraction of their energy. The center-of-momentum energy at the moment of the interaction can therefore be recovered from the measured proton energy. Three Si detectors placed at angles of 7.5° , 22.5° and 37.5° with respect to the beam axis (corresponding to backward angles for elastic

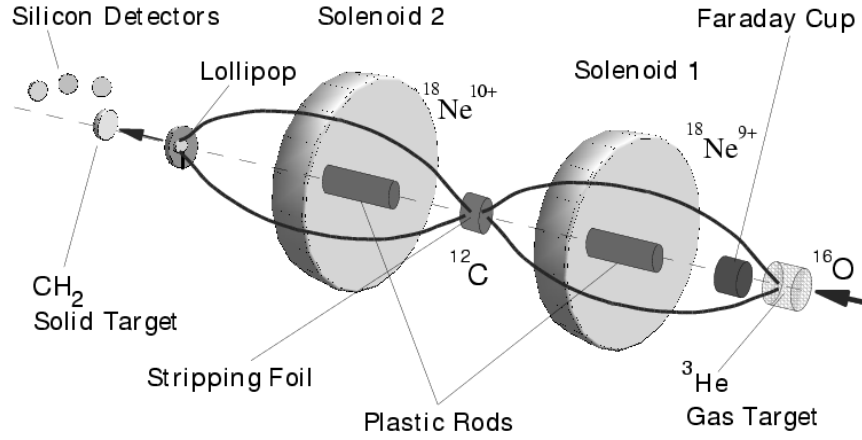


FIG. 1: The experimental setup with beam trajectories through TwinSol. The "lollipop" reduces contamination of the beam by intercepting ions that focus at a different location relative to the ^{18}Ne beam.

scattering of ^{18}Ne on protons) were used to detect recoil protons. The primary ^{16}O beam was pulsed with a repetition rate of 5 MHz and a pulse width of approximately 2 ns. The 5.6 m distance from the primary target to the array of silicon detectors was adequate to obtain a clean separation of the protons associated with the interaction of ^{18}Ne ions in the target from protons associated with elastic scattering of beam contaminants and reactions of other beam isotopes in the target (see Fig. 2). Spectra of protons (in the laboratory frame) measured in the three detectors are shown in Fig. 3. Measurements with a thick natural carbon target were performed to subtract the background associated with carbon in the polyethylene target. The thickness of the carbon target was matched to that of the polyethylene target in terms of proton energy losses. The shaded areas in Fig. 3 show the contributions from reactions of ^{18}Ne on the carbon target.

Proton spectra taken at three different angles, converted to the c.m. system, are shown in Fig. 4. In the conversion of raw spectra to the absolute cross section we used the measured ratio of ^{18}Ne to the intensity of the primary beam ^{16}O . The kinematic relations and energy losses of protons in the target were taken into account in the transformation to the

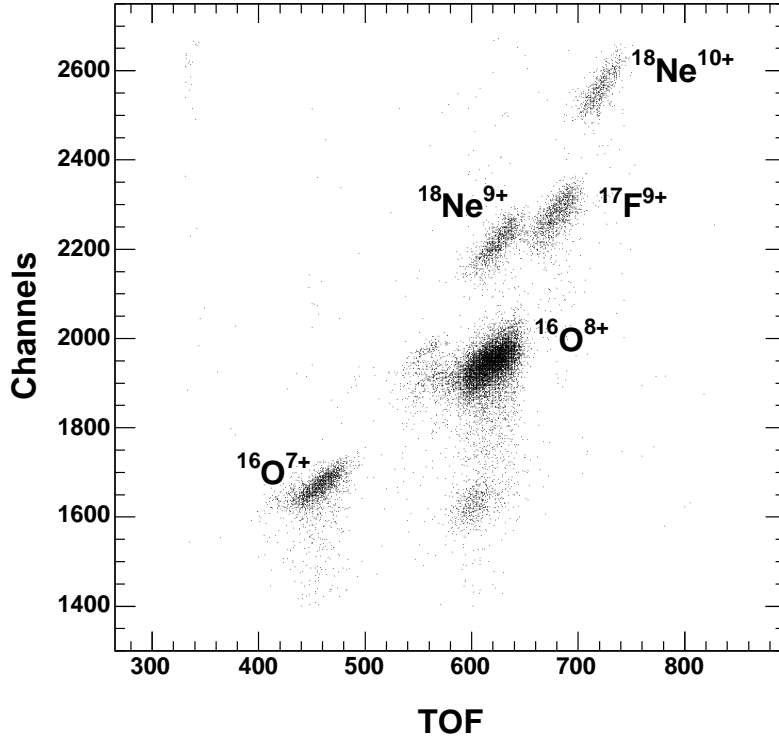


FIG. 2: Composition of the radioactive beam measured by a Si detector placed at the secondary target position. The energy of the ions is shown versus the time of flight (ToF). The “Start” signal for the ToF measurements was produced by the Si detector, and the “Stop” signal was derived from the radiofrequency (RF) signal of the buncher.

c.m. excitation functions. Monte Carlo simulations of the experimental energy resolution were performed for several excitation energies and angles. The typical experimental resolution at 165° was found to be about 30 keV at c.m. energies above 1 MeV. The precision of the excitation energies is about 20 keV, defined mainly by the uncertainties in the specific energy losses of ^{18}Ne ions in the CH_2 target. The absolute cross section values are obtained with uncertainties of 15%. Only one resonance was observed in the $^{18}\text{Ne}+p$ elastic-scattering excitation function in the measured energy range up to 2.7 MeV. This resonance was previously reported in [2] and [4]. We confirm the $1/2^+$ spin-parity assignment for the resonance. The interference pattern of the $l = 0$ resonance phase-shift with Coulomb phase-shift and the angular distribution (three different angles were measured) provides for

unique spin-parity assignment $1/2^+$ for the observed resonance. The excitation energy and width of this state were obtained in an R -Matrix fit: $E_{ex} = 0.74 \pm 0.03$ MeV and $\Gamma = 130 \pm 50$ keV. Statistical uncertainties dominate the reported errors. The parameters of the resonance are in agreement with the results obtained for this state in [2]. Continuum Shell Model (CSM) calculations [7], performed for a chain of oxygen isotopes, predict that the $1/2^+$ second excited state in ^{19}O (the mirror of the observed state in ^{19}Na) has an almost pure ($\approx 70\%$) single particle nature. We need a proper determination of the single particle spectroscopic factor for this resonance to test the predictions of the CSM. Often, the Wigner limit $\gamma_W^2 = \frac{3\hbar^2}{2\mu r^2}$ is used to estimate the single particle width of the resonance and to extract a spectroscopic factor. However, this approach gives only an order-of-magnitude estimate. When applied to the observed $1/2^+$ state, a misleading result is obtained. In particular, the single particle spectroscopic strength extracted for the state is only 25% [2]. In this work, we use the potential-model approach instead. In this case, the properties of the $^{18}\text{Ne}+p$ system are described by a spherical Woods–Saxon potential. If the parameters of the potential are known, then one can predict the properties of the single particle states. The width of the states calculated with the proper potential can then be compared with the experimental values and the spectroscopic factor can be extracted as the ratio of experimental width to the calculated value (as long as only one decay channel is open, as is the case in the energy region of interest). The same approach was adopted in [4] but no details on the potential parameters are given. The initial parameters of the Woods–Saxon potential were found by fitting the excitation energies of the lowest $5/2^+$, $1/2^+$, and $3/2^+$ levels in ^{17}O and ^{17}F simultaneously [8]. It is known that these states are pure single particle in nature. (The Spectroscopic Factors (SF) are 0.9, 0.9 and 1.25, respectively, [9]). A single set of Woods–Saxon potential parameters generates correct energies for the ground and the first two excited states in both ^{17}O and ^{17}F to within 100 keV. The optimum parameters are shown in the table I. The width of the $3/2^+$ state (the only unbound state among the three in $^{17}\text{O}/^{17}\text{F}$) calculated with the potential given in the table I is 90 keV for ^{17}O and 1.14 MeV for ^{17}F , [9]. The experimental values are 95 keV and 1.5 MeV, respectively. The ratio of the experimental to the calculated width gives the spectroscopic factor, which is greater than one for both ^{17}O and ^{17}F . To avoid this, we could increase the diffuseness of the potential (as it was suggested in [8]) to get SF=1.0 for $3/2^+$ instead of 1.25. But since we want to keep all potential parameters the same for $^{17}\text{O}/^{17}\text{F}$ and $^{19}\text{O}/^{19}\text{Na}$ (except V_0), we decided

TABLE I: Parameter of the Woods–Saxon potential

Parameter	$^{17}\text{O} / ^{17}\text{F}$	$^{19}\text{O} / ^{19}\text{Na}$
V_0	-55.77	-50.12
V_{0sl}	6.40	6.40
r_0	1.21	1.21
r_{0sl}	1.21	1.21
r_{Coul}	1.21	1.21
a	0.65	0.65
a_{sl}	0.65	0.65

to use standard values. A potential with the same Woods–Saxon parameters (except for V_0 parameter) was used to calculate the widths and excitation energies of the single particle states in ^{19}O . The potential was adjusted to fit the position of the first $1/2^+$ state in ^{19}O which has pure single particle structure [10] (see Table I). The excitation energy of the other pure single particle state ($3/2^+$ at 5.45 MeV) was reproduced by this potential with an accuracy of 40 keV. The potential model predicts the width of this latter state to be 330 keV, which is consistent with the experimental value of 320 ± 25 keV [10]. The ground state of ^{19}O appears to be underbound by 500 keV, but it is known from shell model calculations [7] and also from experiment [10] that the ^{19}O ground state has significant admixtures from configurations other than simple $(d_{5/2})^3$ for the neutrons in excess of $N = 8$. Thus, our potential model is not adequate for a description of the ground state of ^{19}O . The potential obtained in the procedure described above can now be used to calculate the single-particle width of the $1/2^+$ state in ^{19}Na . It was found that the predicted width of this state is 134 keV, in comparison with the experimental value of 130 ± 50 keV gives a clear indication that it is a pure single particle state ($\text{SF} = 0.95 \pm 0.3$). The spectroscopic factor defined in this way is in very good agreement with the result of CSM which gives 70% SF and a width for the $1/2^+$ resonance in ^{19}Na of about 94 keV (obtained as follows: the single particle width from potential model was multiplied by SF given by CSM). The excitation function for $^{18}\text{Ne}+p$ elastic scattering can be calculated using the potential with the parameters given in the table I. The dashed curve in Fig. 4 shows the result of such a calculation and it is almost identical to the R -matrix fit, shown with the solid curve.

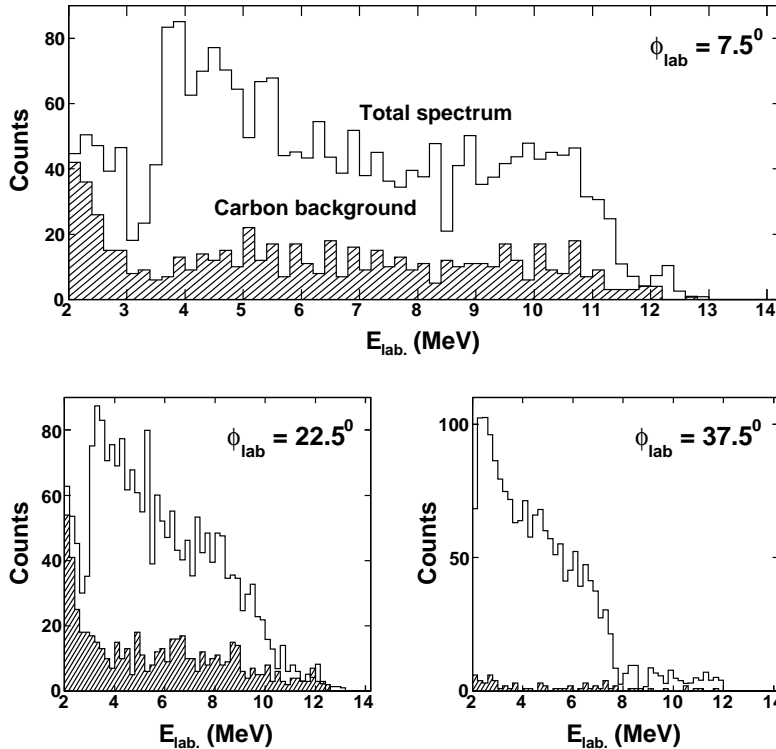


FIG. 3: The spectra of protons from the polyethylene target observed in Si detectors placed at 7.5° , 22.5° and 37.5° in the laboratory frame. The shaded areas represent the proton spectra measured with a natural carbon target. The spectra were gated only on the ToF signal of the $^{18}\text{Ne}^{10+}$ beam (see Fig. 2).

The same procedure can be used to obtain the SF of the $1/2^+$ state from the experimental data of [2] by Angulo et al., where the low-energy part ($E_{cm} \leq 1.4$ MeV) of the $^{18}\text{Ne}+p$ elastic scattering excitation function was measured. The width of the $1/2^+$ state was found to be $\Gamma = 100 \pm 8$ keV [2]. (The error bars include the uncertainty in the arbitrary choice of the channel-radius parameter in the R -matrix fit). The fit to the data from [2] and our potential model gives a spectroscopic factor of 0.75 ± 0.06 . The error reflects the statistical uncertainty of the data from [2]. The state observed at 2.37 MeV in ^{19}O does not manifest itself in the measured excitation function. Nevertheless, conclusions can be drawn from the fact that we did not see any indications of the presence of this state in our data. Specifically, this state is either very narrow and/or only weakly populated in the elastic channel. The

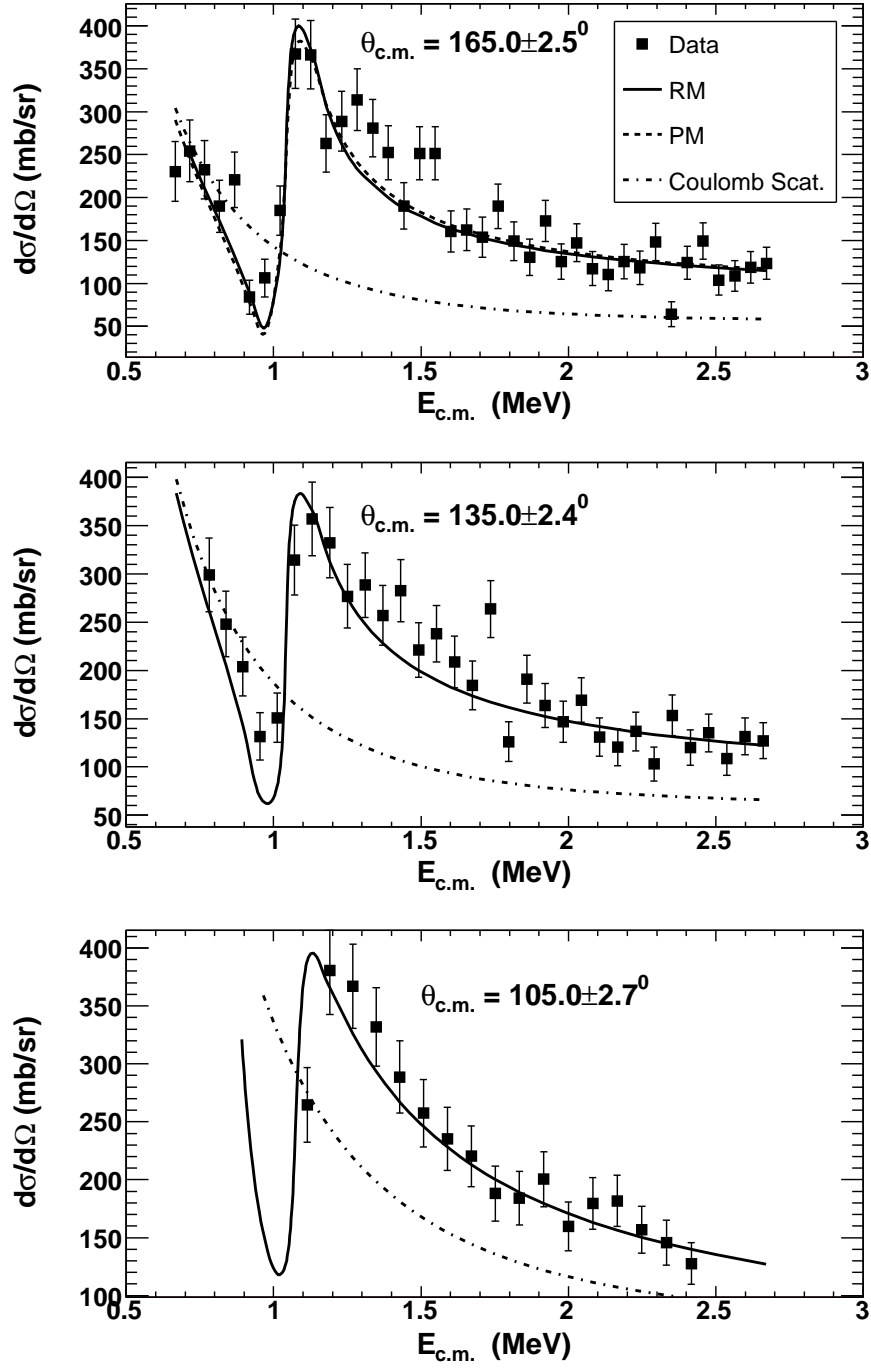


FIG. 4: The excitation functions for $^{18}\text{Ne}+p$ elastic scattering. The solid curves correspond to R -Matrix calculations, the dashed curve(only top figure) to potential-model calculations, and the dashed-dotted curve to Coulomb scattering.

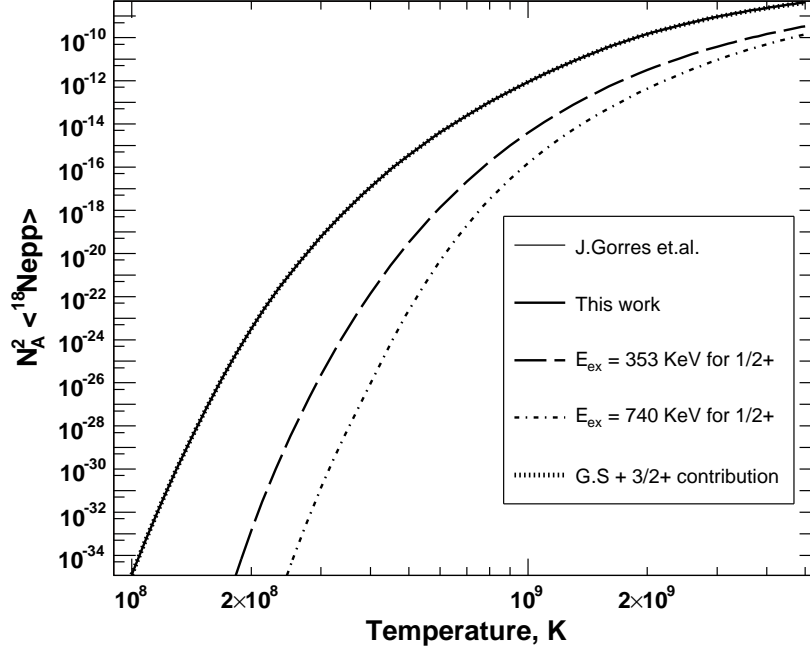


FIG. 5: The reaction rate for two-proton capture $^{18}\text{Ne}(2p,\gamma)$. The calculations were performed in nonresonant and resonant analytical approach used in [6]. The thin, thick and the slashed lines overlaps among each other which show reaction rate for two proton capture on ^{18}Ne which includes the contribution from ground state ($5/2^+$ in ^{19}Na) and the first two excited states ($3/2^+$, $1/2^+$ in ^{19}Na) except slashed line in which excluded contribution from $1/2^+$ state in ^{19}Na . Dashed and dot-dashed lines present contribution from the $1/2^+$ level to the two-proton capture with old and new position of $1/2^+$ levels, respectively.

CSM calculations indicate that the third excited state of $^{19}\text{O}/^{19}\text{Na}$, is built predominantly on the first and the second excited states of $^{18}\text{O}/^{18}\text{Ne}$, and has a spin-parity of $9/2^+$. The width of this state in ^{19}Na , according to the CSM prediction [7] is 1.1 eV. However, this model does not take into account possible admixtures from $g_{9/2}$ shell (only sd shell is included). The single-particle width of this state calculated with the potential given in Table I is 0.5 keV. So even if we assume the 10% admixture of the $g_{9/2}$ shell to the wave function of this state the width would become ~ 5 eV. Much too narrow to be measured in the present work. Hence, the absence of the state around 2.4 MeV (excitation energy) in the observed $^{18}\text{Ne}+p$ spectrum lends indirect support to the prediction of the CSM regarding the nature of this state.

In [4], two peaks with cross sections of ≈ 300 mb/sr were observed at cm energies of 2.4 and 3.1 MeV in the excitation function of $^{18}\text{Ne}+p$ elastic scattering. As shown in Figure 4 no peak is present at 2.4 MeV in our spectrum. It is a clear experimental proof that peaks observed in [4] are not related to the ^{19}Na states populated in elastic scattering. Authors of [4] argue that these peaks can be related to the sequential 2p-decay of the highly excited states of ^{19}Na . Absence of these peaks in our spectrum lends indirect support to this hypothesis because due to lower initial ^{18}Ne beam energy in our experiment these highly excited states would not be populated and thus the peaks at 2.4 MeV and 3.1 MeV cannot be observed.

Potential model with potential parameters given in Table I reproduces excitation energies (with 100 keV accuracy) and widths of all states of single particle nature in ^{17}F , ^{17}O and ^{19}O . It also gives a very good description of the $^{18}\text{Ne}+p$ excitation function up to 2.7 meV (c.m.) (dashed curve in Fig. 4a). Using this model one can make a prediction for the excitation energy and width of the $3/2^+$ ($1d3/2$)¹ single particle state in ^{19}Na . According to our calculations it should have an excitation energy of 5.2 meV and width of ~ 2 meV. This state is the analog of the known 5.45 meV $3/2^+$ single particle state in ^{19}O [9]. It is also a feature of both CSM calculations [7] and shell-model calculation using code Oxbash [11] with the WBT [12] interactions where it appears at 5.53 meV. Thus this state should clearly be in accessible range of [4] where the excitation function was measured up to 5.7 meV. However, we saw no indication of this state. It would be of great interest to locate this state in ^{19}Na in future measurements or understand the reason for its disappearance.

It was shown in [6] that for high temperature and density conditions, two-proton capture on ^{18}Ne will compete with (α, p) and β^+ decay rate. Such stellar condition would allow a fast depletion of ^{18}Ne and a fast leakage out of the hot CNO cycle toward higher masses. In [6], the second excited state $1/2^+$ in the ^{19}Na nucleus, was not known. The position of the $1/2^+$ state was estimated from Thomas–Ehrman shift relative to the mirror $1/2^+$ state in ^{19}O and the value $E_{ex} = 0.353$ meV was used. It is more than two times lower than the experimental value obtained by us and as a result some changes in reaction rates may occurs. We recalculated the $^{18}\text{Ne}(2p, \gamma)$ reaction rate for the same stellar conditions as in [6]. For the case discussed here, the approach proposed in [13] can be used. Using the obtained energy of the $1/2^+$ state, the $^{18}\text{Ne}(2p, \gamma)$ reaction rate was reduced by a factor of 100 due to the new location of the $1/2^+$ resonance (Fig. 5, the ordinate represents total two proton

reaction rate on ^{18}Ne). However, the total reaction rate is almost unaffected since at stellar temperatures, the reaction rate is dominated mostly by g.s. and first excited state.

III. CONCLUSION

The structure of the proton-rich particle unstable nucleus ^{19}Na was investigated in the excitation energy region from 0.5 meV to 2.7 meV by means of resonance elastic scattering of a radioactive beam of ^{18}Ne on protons. Only one state, at an excitation energy of 0.74 meV, was observed. Its spin and parity were confirmed to be $1/2^+$. A potential model approach was used to obtain the single particle spectroscopic factor of this resonance. We show that the state has a reasonably pure single-particle structure $(2s1/2)^1$, in agreement with shell-model calculations [7]. The absence of another low-lying state (observed at an excitation energy of 2.37 meV in the mirror nucleus ^{19}O) in the $^{18}\text{Ne}+p$ excitation function is indirect confirmation of the shell-model prediction that this is a $9/2^+$ state built on an excited states of ^{18}Ne . As such, it would be very narrow and only weakly populated in elastic scattering.

We did not observe a broad peak at 2.4 meV, found in [4], which indicates that this peak is unrelated to elastic scattering and may be the result of sequential $2p$ decay from the higher lying excited states of ^{19}Na (as argued in [4]). The potential model with potential parameters obtained in this work was used to predict the excitation energy and width of a $3/2^+$ single particle state in ^{19}Na . This state should be well in the range of the experimental data of work [4], but there is no indication of this state. Additional measurements at higher excitation energies (and different angles) are needed to locate this resonance or understand the reason for the disappearance of this state.

The $^{18}\text{Ne}(2p,\gamma)$ astrophysical reaction rate was recalculated using the new experimental information on the excitation energy of the $1/2^+$ state. The $(2p,\gamma)$ reaction rate due to this state is actually 100 times lower than it was suggested in previous work [6], however, due to the fact that the $^{18}\text{Ne}(2p,\gamma)$ reaction at stellar temperatures is dominated by the ground and the first excited state this finding did not make significant impact on the total reaction rate.

IV. ACKNOWLEDGEMENTS

This work was supported by National Science Foundation under Grant numbers PHY01-40324, PHY02-44989 and PHY01-39950. The authors are grateful to V.Goldberg, J.Görres, A.Volya and M.Wiescher for useful discussions and comments.

- [1] J. Cerny *et al.*, Phys. Rev. Lett. 22, 612 (1969).
- [2] C. Angulo *et al.*, Phys. Rev. C67 014308 (2003).
- [3] M. Y. Lee *et al.*, Nucl. Instrum. Methods, A 422 536 (1999).
- [4] F. Oliveira, *et al.*, Eur. Phys. J. A 24, 237 (2005).
- [5] K. P. Artemov *et al.*, Sov. J. Nucl. Phys. 52, 406 (1990).
- [6] J. Gorres *et al.*, Phys. Rev. C 51 392 (1995).
- [7] A. Volya *et al.*, Phys. Rev. Lett. 94, 052501 (2005). A. Volya, Private Communication.
- [8] V. Z. Goldberg *et al.*, Phys. Rev. C 69 031302(R)(2004).
- [9] D. R. Tilley, Nucl. Phys. A 564 1 (1993).
- [10] D. R. Tilley Nucl. Phys. A 595 1 (1995).
- [11] B. A. Brown *et al.*, MSU-NSCL report No. 524 (1986).
- [12] E. K. Warburton *et al.*, Phys. Rev. C 46 923 (1992).
- [13] W. A. Fowler *et al.*, Annu. Rev. Astron. Astrophys. 5 525 (1967).